

## Supporting Information

### Scalable and highly efficient high temperature solar absorber coatings based on high entropy alloy nitride AlCrTaTiZrN with different antireflection layers

Cheng-Yu He<sup>a,b</sup>, Xiang-Hu Gao<sup>a,b\*</sup>, Dong-Mei Yu<sup>a,b</sup>, Xiao-Li Qiu<sup>c</sup>, Hui-Xia Guo<sup>d</sup>, Gang Liu<sup>a,b\*</sup>

<sup>a</sup> *Research and Development Center for Eco-Chemistry and Eco-Materials, State Key Laboratory of Solid Lubrication, Lanzhou Institute of Chemical Physics, Chinese Academy of Sciences, Lanzhou 730000, China*

<sup>b</sup> *Center of Materials Science and Optoelectronics Engineering, University of Chinese Academy of Sciences, Beijing 100049, China*

<sup>c</sup> *College of physics and engineering, Chengdu normal university, Chengdu 611130, China*

<sup>d</sup> *Key Laboratory of Bioelectrochemistry & Environmental Analysis of Gansu Province, College of Chemistry & Chemical Engineering, Northwest Normal University, Lanzhou 730070, P. R. China*

---

\* Corresponding author:  
E-mail address: [gaoxh@licp.cas.cn](mailto:gaoxh@licp.cas.cn) (Xiang-Hu Gao)  
[gangliu@licp.cas.cn](mailto:gangliu@licp.cas.cn) (Gang Liu)

## 1. Experimental details

Single layer high entropy alloy nitride (AlCrTaTiZrN) based SSSACs were fabricated on stainless steel (SS) and silicon substrates via reactive RF magnetron sputtering. For an aim to optimize deposition process, individual layers (AlCrTaTiZrN and SiO<sub>2</sub>/Si<sub>3</sub>N<sub>4</sub> layers) were deposited on a variety of substrates such as SS, Si and BK7 glass substrates (the Si substrates were employed to measure SEM images, the glass substrates were used for the extraction of optical constants, the SS substrates were employed to estimate optical properties and thermal stability of the proposed coating). Firstly, ultrasonic cleaning of the SS substrates was performed in acetone, deionized water and alcohol for 15 min successively. High entropy alloy AlCrTaTiZr target was synthesized by powder metallurgy. Equi-molar Al, Cr, Ta, Ti and Zr powders were completely mixed, and then were placed in a sheath working as a mold ultimately undergoing sintering hot extrusion. The as-synthesized target with a disk of 76.2 mm in diameter and 8 mm in thickness is used to prepare high entropy alloy nitride AlCrTaTiZrN layer under the Ar/N<sub>2</sub> flow rate of 28/2 sccm. By adjusting deposition time, the thickness of AlCrTaTiZrN film will vary. A highly pure Si target (purity 99.9%) is used to fabricate the antireflection layer. Wherein, SiO<sub>2</sub> layer was prepared with the mixture Ar/O<sub>2</sub> flow rate of 28/8 sccm, Si<sub>3</sub>N<sub>4</sub> was deposited with the mixture Ar/N<sub>2</sub> flow rate of 28/25 sccm. Thus, novel AlCrTaTiZrN/SiO<sub>2</sub> and AlCrTaTiZrN/Si<sub>3</sub>N<sub>4</sub> coatings were successfully deposited on SS substrate. Before the deposition, the chamber was pumped down to a 5×10<sup>-6</sup> mTorr pressure. In order to obtain reflectance (R) and (T), single AlCrTaTiZrN, SiO<sub>2</sub> and Si<sub>3</sub>N<sub>4</sub> films were prepared on glass substrates with identical deposition parameters. Optical constants of individual layers are subsequently calculated by fitting the measured R and T spectra using coating design (CODE) software.

The reflectance (R) and transmittance (T) spectra (0.3-2.5 $\mu\text{m}$ ) of high entropy alloy nitride AlCrTaTiZrN based coating were obtained by a Perkin Elmer Lambda 950 UV/Vis/NIR Spectrometer. The reflectance spectra (2.5-25  $\mu\text{m}$ ) of the coating were measured on a Bruker TENSOR 27 FT-IR Spectrometer. The coatings were heat-treated under vacuum in a tubular furnace at temperatures in the range of 500-900  $^{\circ}\text{C}$  for 2 h with a pressure of  $5.0 \times 10^{-1}$  Pa. High vacuum environment was generated using a Pfeiffer turbopump. The accuracy of the set temperature was  $\pm 1$   $^{\circ}\text{C}$ . Annealing involved increasing the temperature to the desired temperature at a slow rate of 5  $^{\circ}\text{C}/\text{min}$  and maintaining the desired temperature for the designed time. Subsequently, the samples were naturally cooled down to room temperature. Long term thermal stability test is carried out at 650  $^{\circ}\text{C}$  for sample O and 600  $^{\circ}\text{C}$  for sample N. Firstly, the samples were annealed at 600 $^{\circ}\text{C}$  or 650  $^{\circ}\text{C}$  for 10 h, then restored room temperature to measure the values of solar absorptance and thermal emittance. Subsequently, the samples were heated to 600 $^{\circ}\text{C}$  or 650  $^{\circ}\text{C}$  again for 50 h, then restored room temperature to obtain the values of solar absorptance and thermal emittance. The values of solar absorptance and thermal emittance after annealing for 100 h, 200 h and 300 h were captured using same method. The scanning electron microscopy (SEM) is carried out to explore surface and cross-sectional topography. The X-ray diffraction (XRD) (Rigaku D/max2400 PC, Tokyo, Japan) with Cu K $\alpha$  radiation operating at 40 kV and 200 mA was employed to measure phases of the SSSACs before and after annealing at different temperatures. The Raman spectrometer (Renishaw inVia) was used to obtain Raman spectra, which was kept at room temperature using a 532 nm laser as the excitation source.

## **2. Optical models**

## 2.1 AlCrTaTiZrN layer

Many transition metal nitrides show the characteristic of metallic materials. As a result, the optical properties of AlCrTaTiZrN layer can be described by choosing the Drude model<sup>1</sup>. The OJL model represents the band gap transitions in the ultraviolet and visible spectral range, for which the parabolic bands are assumed with tail states exponentially decaying into the band gap<sup>2</sup>. The Kim model is an extension of the simple harmonic oscillator for vibrational modes, which allows a continuous shift of the line shape between a Gaussian and a Lorentzian profile<sup>3</sup>. The dielectric function is given in Eq. (1):

$$\epsilon_{\text{AlCrTaTiZrN}} = \epsilon_{\text{background}} + \epsilon_{\text{Drude}} + \sum \epsilon_{\text{Kim}} + \epsilon_{\text{OJL}} \quad (1)$$

## 2.2 Si<sub>3</sub>N<sub>4</sub> layer

The Si<sub>3</sub>N<sub>4</sub> acting as antireflection film shows the dielectric properties. The Si<sub>3</sub>N<sub>4</sub> has strong ultraviolet and infrared absorptions, which are caused by the interband electronic transitions and the excitation of vibrational quanta, respectively<sup>4</sup>. The dielectric function model of the Si<sub>3</sub>N<sub>4</sub> layer includes Tauc-Lorentz model and a sum of Brendel models, as given by Eq. (2):

$$\epsilon_{\text{Si}_3\text{N}_4} = \epsilon_{\text{background}} + \epsilon_{\text{Tauc-Lorentz}} + \sum \epsilon_{\text{Brendel}} \quad (2)$$

The Brendel oscillator model for vibrational modes is the improvement on the simple harmonic oscillator model<sup>5</sup>. Tauc-Lorentz model is an interband transition model that is used to account for ultraviolet absorption.

## References

[1] S. Zhao, *Sol. Energy Mater. Sol. Cells*, 2006, **90**, 1861-1874.

- [2] L. Rebouta, P. Capela, M. Andritschky, A. Matilainen, P. Santilli, K. Pischow, E. Alves, *Sol. Energy Mater. Sol. Cells*, 2012, **105**, 202-207.
- [3] L. Zheng, F. Gao, S. Zhao, F. Zhou, J.P. Nshimiyimana, X. Diao, *Appl. Surf. Sci.*, 2013, **280**, 240-246.
- [4] Y. Wu, C. Wang, Y. Sun, Y. Xue, Y. Ning, W. Wang, S. Zhao, E. Tomasella, A. Bousquet, *Sol. Energy Mater. Sol. Cells*, 2015, **134**, 373-380.
- [5] Y. Ning, W. Wang, L. Wang, Y. Sun, P. Song, H. Man, Y. Zhang, B. Dai, J. Zhang, C. Wang, Y. Zhang, S. Zhao, E. Tomasella, A. Bousquet, J. Cellier, *Sol. Energy Mater. Sol. Cells*, 2017, **167**, 178-183.

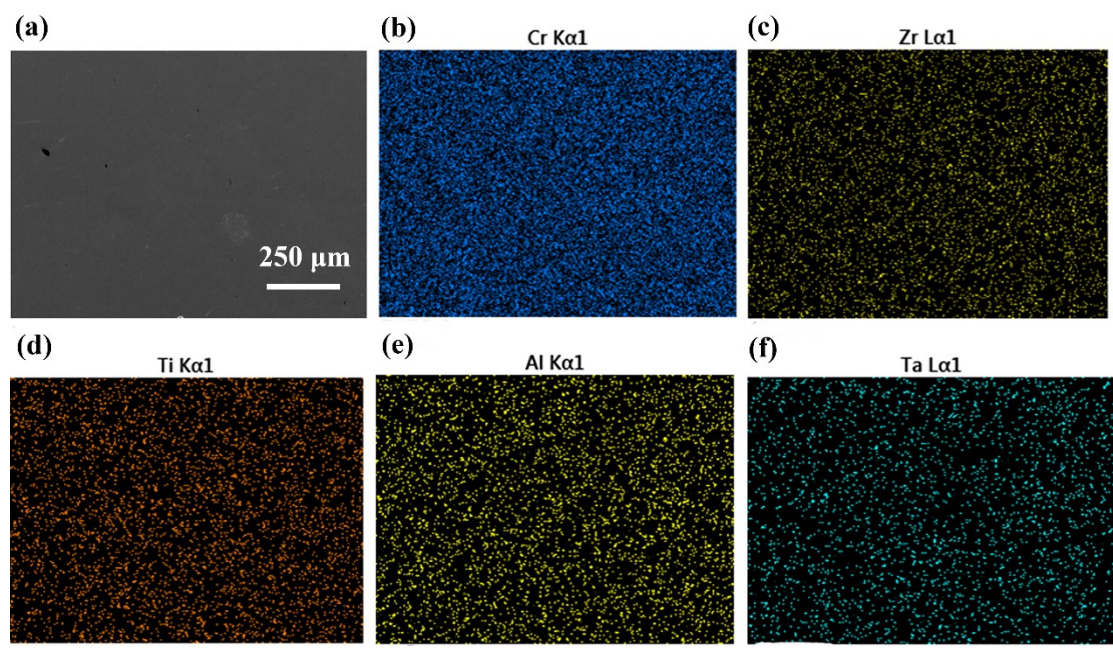


**Fig. S1** Microstructure and element distribution of the AlCrTaTiZrN layer deposited on SS substrates: (a) surface SEM image; (b-f) EDS elemental maps of the region.

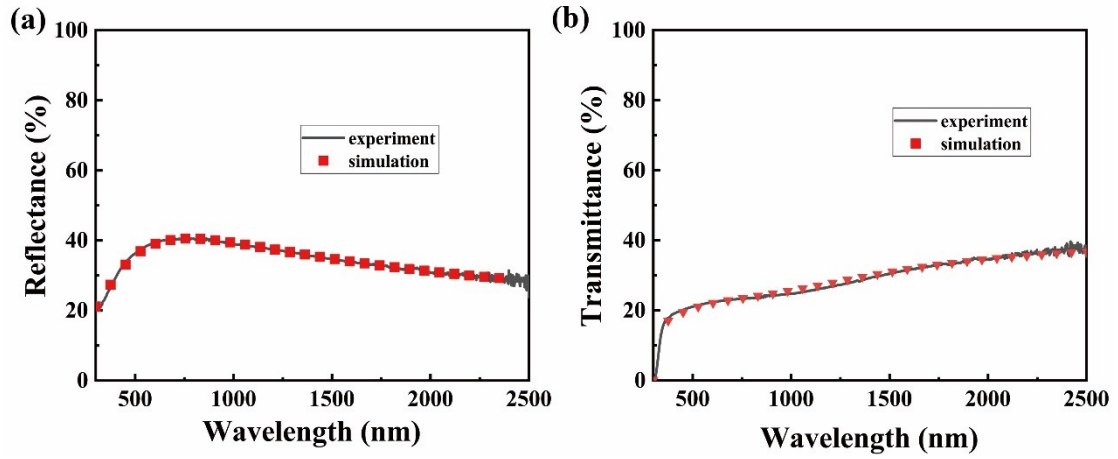


**Fig. S2** Experimental and simulated R (a), T (b) spectra of the AlCrTaTiZrN film deposited on glass substrates.

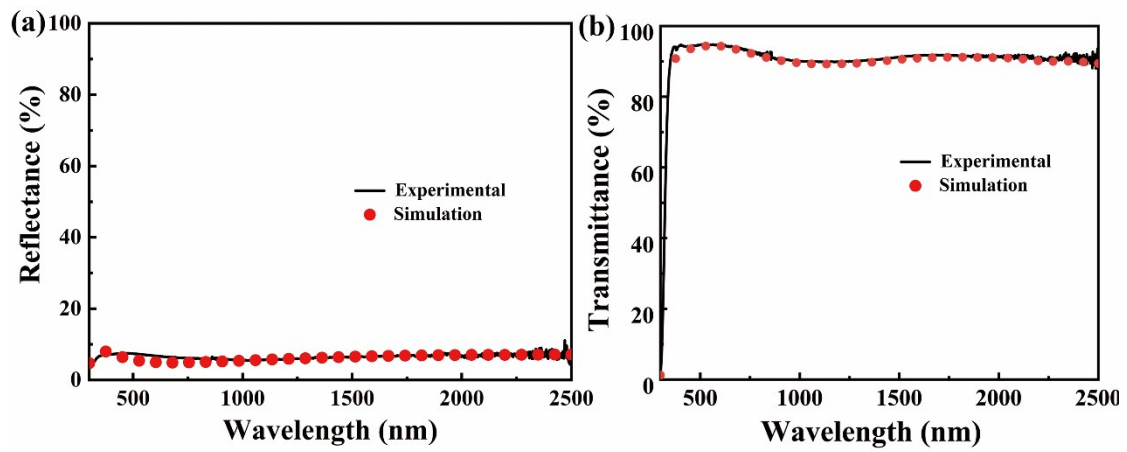


**Fig. S3** Experimental and simulated (a) R, (b) T, spectra of the SiO<sub>2</sub> film deposited on glass substrates.



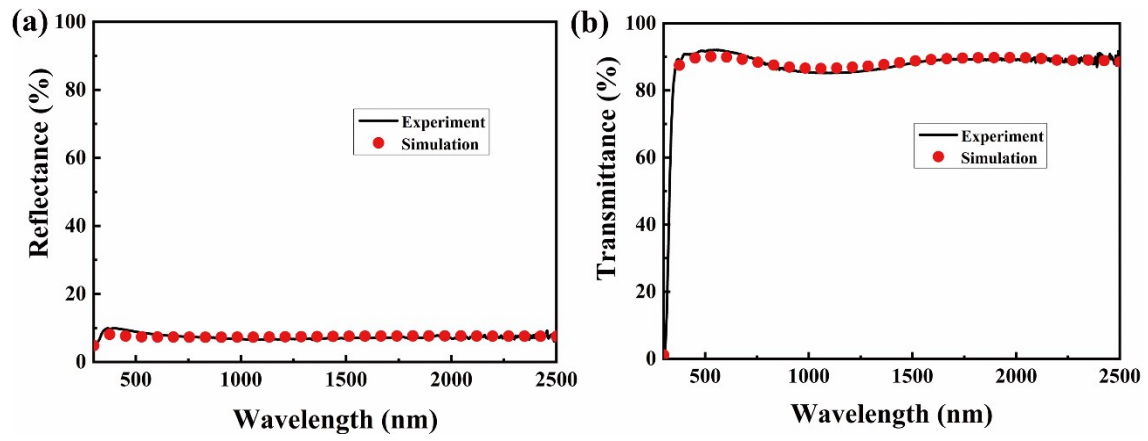


**Fig. S4** Experimental and simulated (a) T, (b) R, spectra of the  $\text{Si}_3\text{N}_4$  film deposited on glass substrates.

**Table S1.** The deposition parameters of the AlCrTaTiZrN, SiO<sub>2</sub> and Si<sub>3</sub>N<sub>4</sub> layers

layer	RF power (W)	N <sub>2</sub> (sccm)	O <sub>2</sub> (sccm)	Ar (sccm)	Thickness (nm)	Deposited time (min)	Operating pressure (Pa)
AlCrTaTiZr N	250	2	0	28	46	6	1.03
SiO <sub>2</sub>	160	0	8	28	88	150	1.28
Si <sub>3</sub> N <sub>4</sub>	150	25	0	28	86	100	1.32

**Table S2** Optical properties of the SS/AlCrTaTiZrN film, sample O and sample N

layer	Absorptance ( $\alpha$ )	Emittance ( $\epsilon$ )	$\alpha/\epsilon$
SS	0.249	0.051	4.9
SS/AlCrTaTiZrN	0.795	0.051	15.6
sample O	0.916	0.051	18.0
sample N	0.928	0.051	18.2

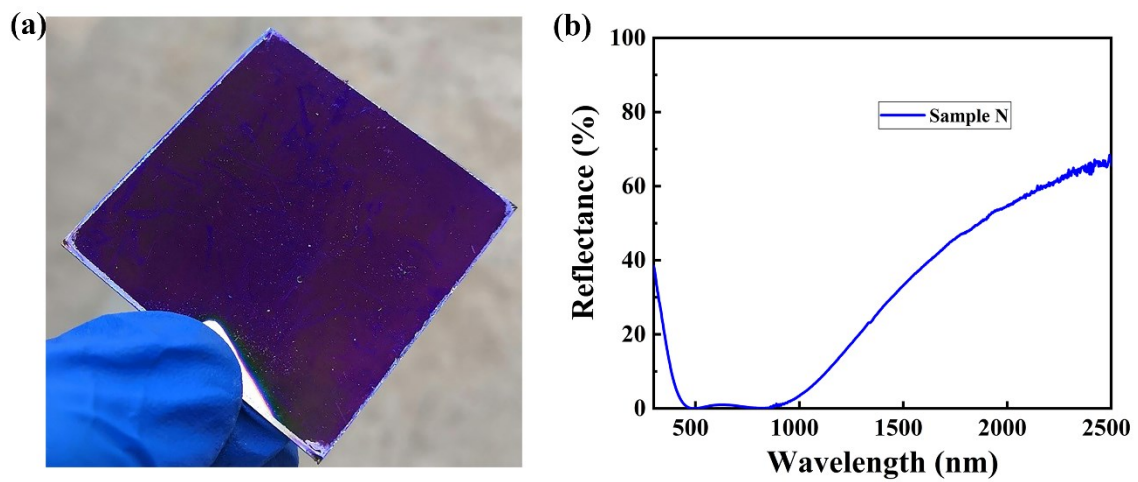


**Fig. S5** (a) Photograph and (b) reflectance spectra of the as-deposited sample N.

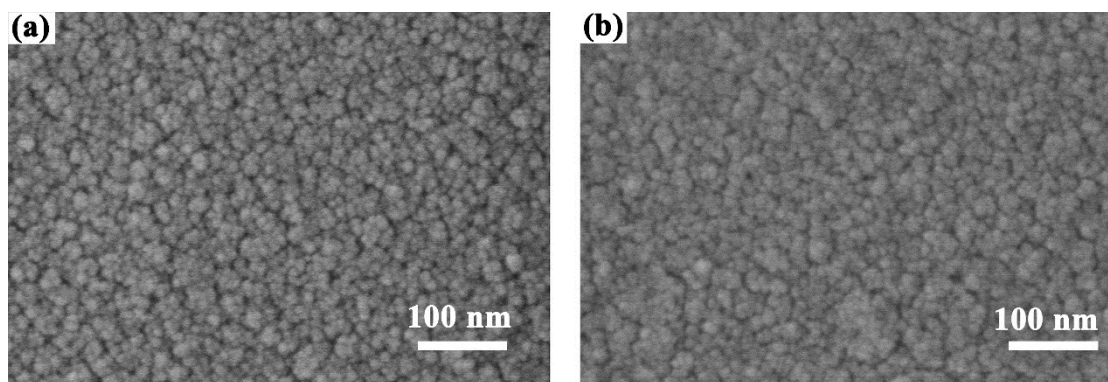


**Fig. S6** Amplified surface SEM images of the pristine (a) sample O and (b) sample N.

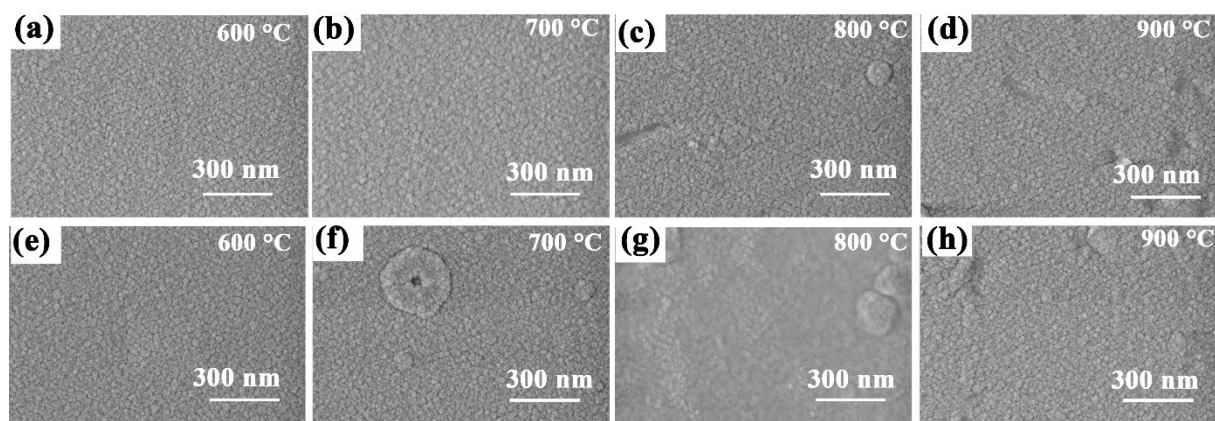


**Fig. S7** Amplified surface SEM images of sample O annealed at (a) 600 °C, (b) 700 °C, (c) 800 °C and (d) 900 °C; Amplified surface SEM images of sample N annealed at (e) 600 °C, (f) 700 °C, (g) 800 °C and (h) 900 °C.

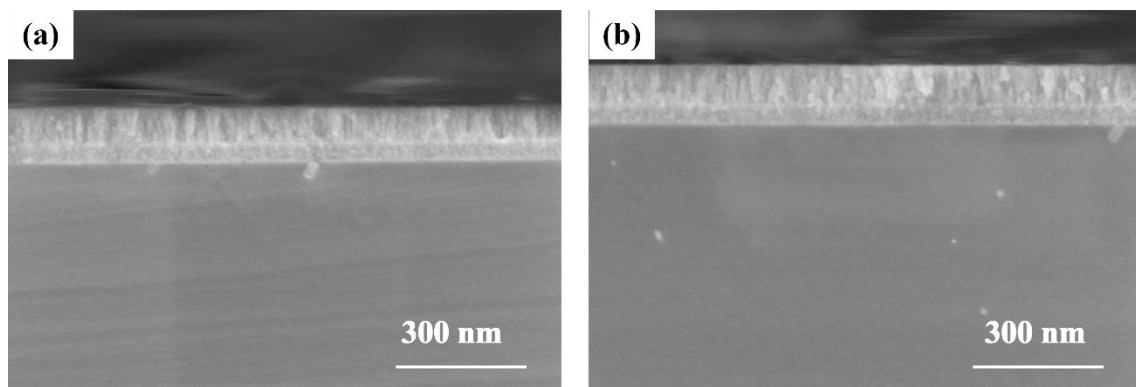


**Fig. S8** Cross-sectional SEM images of (a) sample O and (b) sample N annealed at 900 °C for 2 h.

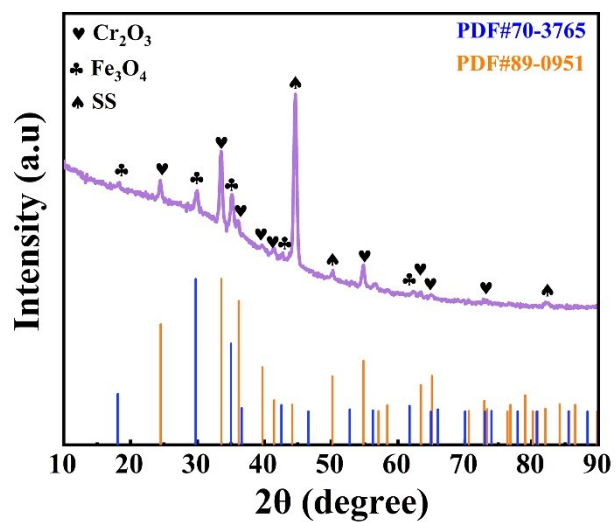


**Fig. S9** XRD patterns of SS substrate after annealing at 900 °C for 2 h



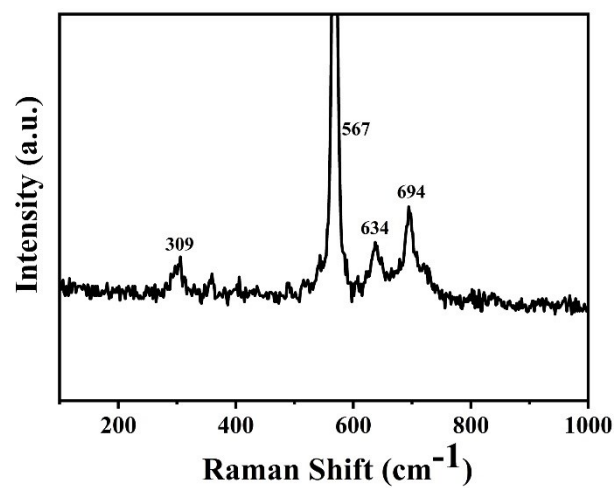


**Fig. S10** Raman spectrum of SS substrates after annealing at 900 °C for 2h

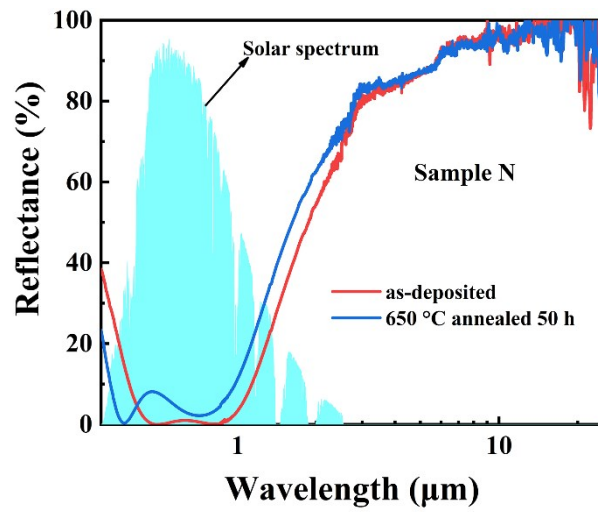


**Fig. S11** The reflectance spectra of the as-deposited coating and the sample annealed at 650 °C for 50 h.

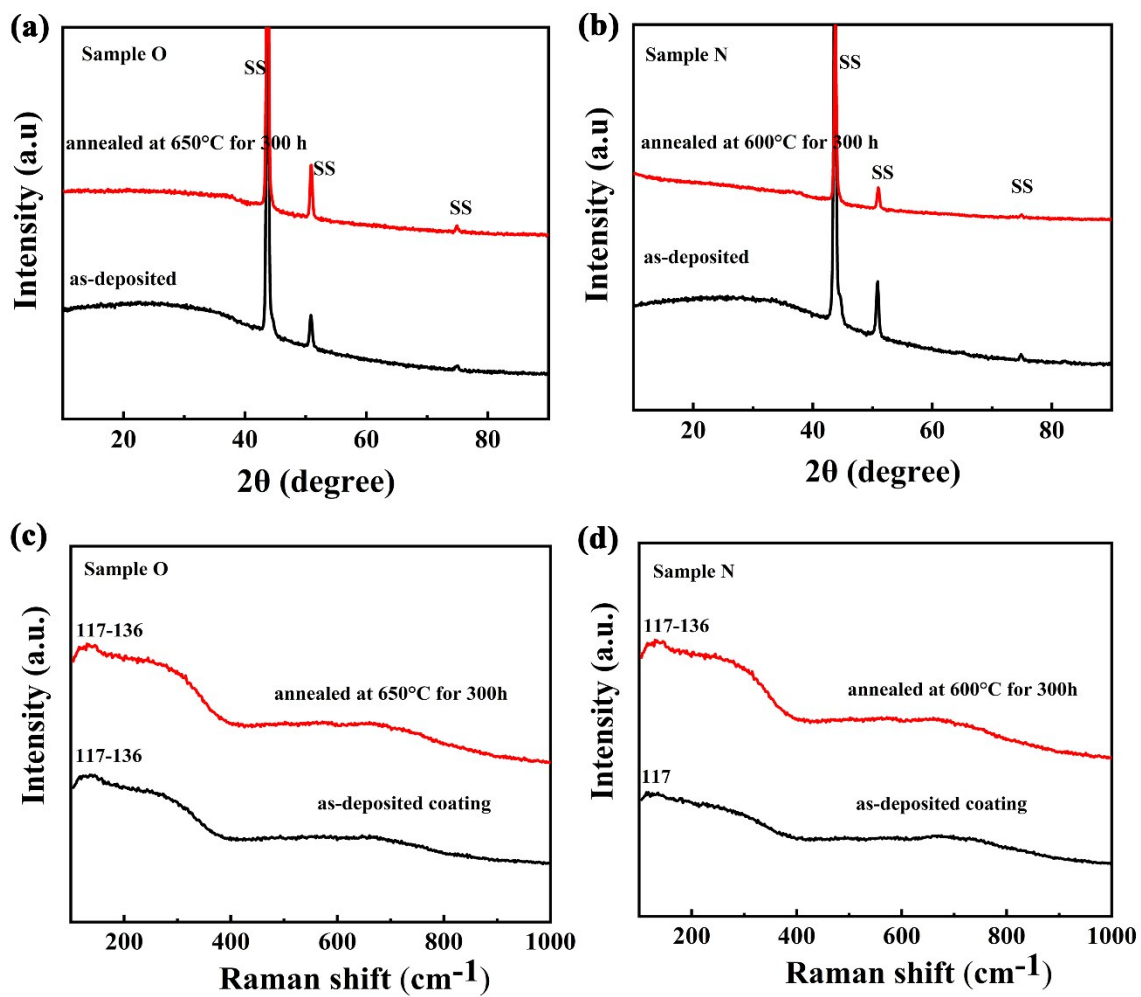


**Fig. S12** XRD patterns of (a) sample O annealed at 650 °C h for 300 h and (b) sample N annealed at 600 °C for 300 h; Raman spectra of (c) sample O annealed at 650 °C h for 300 h and (d) sample N annealed at 600 °C for 300 h.

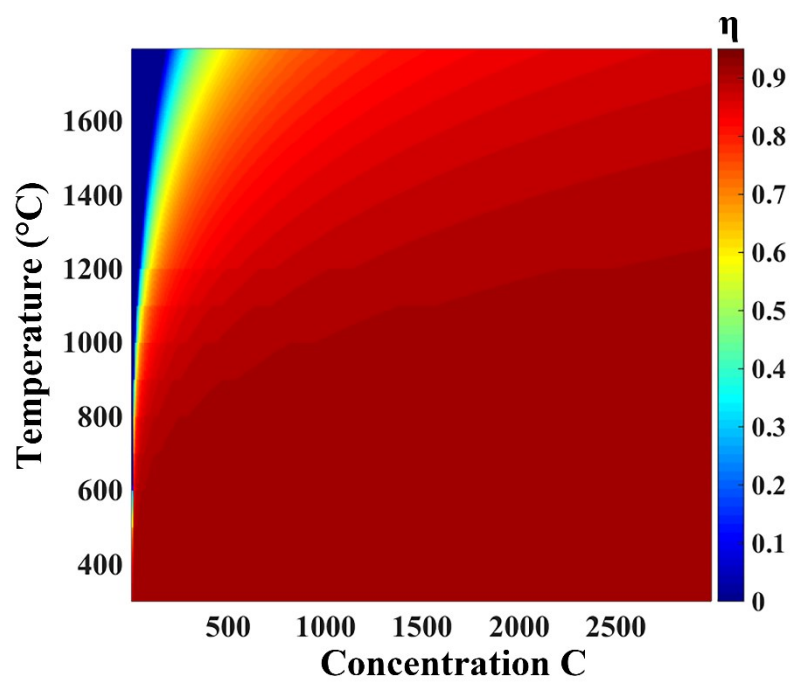


**Fig. S13** Photothermal conversion efficiency of pristine sample O at different concentration radios and different working temperatures.

**Table S3** Thermal emittance of the sample O and sample N at different working temperatures.

Temperature (°C)	sample O	sample N
82	0.051	0.051
400	0.114	0.107
500	0.138	0.130
600	0.163	0.154
650	0.175	0.167
700	0.189	0.180
800	0.215	0.208
850	0.229	0.222
900	0.243	0.237
1000	0.271	0.267